Performance analysis of a high-resolution wide-angle foveated optical system

George Curatu[a] and James E. Harvey[b]

[a]Curatu Optics, 2972 South Tanner Rd, Orlando, FL 32820
[b]University of Central Florida, 4000 Central Florida Blvd, Orlando, FL 32816

ABSTRACT

Optical foveated imaging using liquid crystal spatial light modulators has received considerable attention in the recent years as a potential approach to reducing size and complexity in wide-angle lenses for high-resolution foveated imaging. In this paper we propose a very compact design for an F/2.8 visible monochromatic foveated optical system covering a total field-of-view of 80 degrees and capable of achieving a resolution in excess of 100 MPixels. The diffraction efficiency and image quality of the foveated optical system are estimated. The foveated optical system is compared to equivalent conventional wide-angle lenses in terms of size, complexity and image quality. Fabrication and assembly tolerances as well as limitations of the current transmissive LC SLM technology are taken into consideration.

Keywords: foveated imaging, adaptive optics, wide-angle lenses, aberration compensation, spatial light modulators, liquid crystal devices.

1. INTRODUCTION

The development of compact imaging systems capable of covering a wide field-of-view (FOV) while transmitting high-resolution images in real-time is critical in a variety of military and civilian applications: surveillance, threat detection, target acquisition, tracking, remote operation of unmanned vehicles, etc. Foveated imaging was proposed as a data compression technique to speed up transmission and processing of high-resolution digital video frames by reducing the resolution of the image with the exception of a region of interest (ROI), which can be dynamically repositioned anywhere within the FOV[1,2]. This multiresolution video compression method was inspired by the operation of the human vision apparatus, and is ideal for applications where images from a wide FOV have to be transmitted and processed in real-time, yet high-resolution is required at the ROI. Foveated imaging can be achieved at the software level, by applying foveation algorithms to full-resolution digital video frames from a conventional imaging system[1-3], or it can be achieved at the hardware level, by combining images from several sensors[4,5] or by using sensor arrays with variable resolution[6-8].

Reducing the size and complexity of the optical system is another important task in foveated imaging applications requiring fast (low F/#) and light-weight wide-angle optics. Such lenses are often used in surveillance, navigation of unmanned vehicles, tracking, threat detection, and other applications where a large FOV has to be covered constantly, in different lighting conditions. The large aperture (low F/#) is generally needed to gather more light onto the sensor in outdoors applications, where poor ambient lighting can result in a low SNR and therefore, poor detection capabilities. On the other hand, aberrations in the lens increase quickly with the aperture and the field angle, due to the severe "ray bending." As a result, fast wide-angle lenses typically require complex designs with multiple elements, in order to carefully balance and correct these aberrations[9]. Martinez et al. proposed a compact wide-angle lens with variable resolution across the FOV to reduce the size and complexity of wide-angle optics in foveated imaging systems[10]. The fundamental concept behind the optical foveated imaging technique described by Martinez et al. is reducing the number of elements in a fast wide-angle lens by placing a transmissive phase spatial light modulator (SLM) at the pupil stop to dynamically compensate aberrations left uncorrected by the optical design at preselected points within the FOV. Such hybrid lens would form an aberrated image over its wide FOV with the exception of a highly resolved ROI, which could be dynamically positioned anywhere within the FOV by adjusting the optical path difference (OPD) pattern introduced

Photonic Microdevices/Microstructures for Sensing II, edited by Xudong Fan, Hai Xiao, Anbo Wang,
Proc. of SPIE Vol. 7682, 76820O · © 2010 SPIE · CCC code: 0277-786X/10/$18 · doi: 10.1117/12.850527

by the SLM to correct the wavefront aberration at the desired field angle. A great advantage of the proposed foveated optical system (FOS) is that it could be combined with variable resolution sensors in order to develop compact high-resolution wide-angle foveated imaging systems for applications where light-weight, fast data transmission, and low power consumption are critical requirements.

In the recent years, considerable research and development has been conducted in the area of optical foveated imaging using liquid crystal (LC) SLM technology, and several FOSs have been built[11-16]. However, most research has only been focused so far on the experimental demonstration of the basic principle, using off-the-shelf components, without much concern for the practicality or the optical performance of the systems. In this paper we propose a very compact and practical design for an 18 mm F/2.8 visible monochromatic FOS. The FOS covers a total FOV of 80 degrees and would be capable of achieving a resolution larger than 100 MPixels with a large format sensor array (25 mm diagonal with 1.7 μm pixel pitch). The diffraction efficiency and modulation transfer function (MTF) of the FOS are estimated. The FOS is compared to equivalent conventional wide-angle lenses in terms of size, complexity, and MTF.

2. BACKGROUND

The phase SLM is the key component enabling optical foveated imaging. Phase SLMs are devices used to control the optical wavefront by dynamically changing the OPD across the aperture. Two different types of phase SLMs based on two different technologies have emerged as the most commonly used devices in applications requiring wavefront correction: deformable mirrors (DMs) and LC SLMs. Reflective devices, such as DMs and reflective LC SLMs have been commercially available for many years, and have several advantages over transmissive LC SLMs. For instance, segmented DMs have very good zero-order diffraction efficiencies, large phase strokes, and no dispersion, allowing multispectral applications. In addition, some segmented DMs have elements with piston-tip-tilt correction capabilities to minimize the residual wavefront error[17]. Reflective LC SLMs also offer some advantages over transmissive LC SLMs, since they typically have larger pixel fill factors and smooth transitions between pixels, maximizing the zero order diffraction efficiency[18]. Although reflective devices have been successfully used in slower systems with narrower FOVs, such as telescopes[19-21], typical optical design arrangements in fast wide-angle FOSs pose particular challenges related to placing a reflective SLM at the stop. Systems using reflective devices require a fold in the optical axis after the reflection at the stop. Folded designs are not practical in the case of fast wide-angle systems, since they increase the complexity and size of the system and limit the F/# and FOV.

Currently, transmissive LC SLMs seem to be the only transmissive devices available that could potentially allow the development of practical fast wide-angle FOSs. However, there are several fundamental limitations intrinsic to the current transmissive SLM technology. High-resolution transmissive SLMs are based on the same thin film transistor (TFT) technology used in transmissive liquid crystal displays (LCD). A drawback of this technology is that, when used in transmissive devices, the active area of each pixel is limited by a shadow mask, which is placed over the transistors and the wiring electronics to prevent photoconduction. The shadow mask reduces the SLM pixel fill factor, affecting the diffraction efficiency and the image quality of the FOS. Decreasing the size of the electronics could be a solution to increasing the fill factor in transmissive SLMs, but there are technological limitations to how much further the electronics and shadow mask can be shrunk (2.8 μm seems to be the current minimum mask width achieved in transmissive TFT devices). Another limitation imposed by the transmissive LC SLM technology is the discrete OPD pattern introduced by the SLM, with piston-only correction at each element, which generates a periodic residual wavefront error (RWFE) at every pixel. The RWFE produces a quasi-periodic phase structure that further affects the diffraction efficiency and the image quality of the FOS.

The amount of signal onto the sensor and the image quality are the two most important performance characteristics of an optical imaging system. In the case of FOSs based on transmissive LC SLMs, diffraction is the main factor affecting both of these characteristics at the ROI. A significant diffractive effect is caused by the periodic amplitude gridlike structure created by the shadow mask, which is equivalent to the effect of a two dimensional amplitude grating. Another diffractive effect is caused by the RWFE, which forms a periodic sawtoothlike phase structure with the same period as the amplitude grating, which has the effect of a two-dimensional blazed grating with the blaze angle slowly varying across the pupil. The amplitude and phase diffraction caused by the pixelated structure of the transmissive LC SLMs affects the transmission, the zero order diffraction efficiency, and the image quality of the FOS[22].

3. DIFFRACTION EFFICIENCY AND MTF

Figure 1 shows one-dimensional schematic plots of the pupil amplitude and phase of an FOS based on transmissive LC SLMs after correcting the wavefront aberration at the ROI. Consider the following notation: *a* is the SLM pixel pitch, and *b* is the active pixel width. The amplitude, $t(x)$, has a value of one at the regions where the SLM is transparent and zero where the SLM is opaque. The phase, $\psi(x)$, has the effect of a blazed transmission phase grating with the blaze angle following a similar variation across the pupil as the slope of the corrected wavefront aberration, $W(x)$.

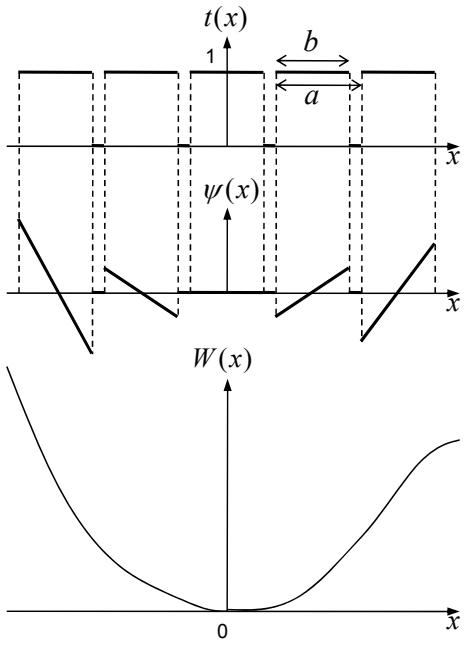

Figure 1: One-dimensional pupil amplitude and phase transmission plots, $t(x)$ and $\psi(x)$, after correcting the aberration $W(x)$.

The local peak-to-valley (P-V) RWFE on *x* and *y* at the pixel *[i, j]* is given by the local slope of the wavefront aberration and the pixel pitch of the SLM:

$$\begin{aligned} RWFE_{P\text{-}Vx}[i,j] &= a \times \left| \frac{\partial W(x,y)}{\partial x} \right|_{x=x_i, y=y_j} \\ RWFE_{P\text{-}Vy}[i,j] &= a \times \left| \frac{\partial W(x,y)}{\partial y} \right|_{x=x_i, y=y_j} \end{aligned} \tag{1}$$

Assuming an FOS with a high-resolution SLM, the RWFE varies relatively slowly over several pixels, so for each order, (m_x, m_y), we can define the local two dimensional diffraction efficiency at every pixel *[i, j]* as the product between the local diffraction efficiencies on *x* and *y*[22]:

$$\sigma_{m_x,m_y}[i,j] = \left(\frac{b}{a}\right)^4 \operatorname{sinc}^2\left[\frac{b}{a}\left(m_x - \frac{RWFE_{P\text{-}Vx}[i,j]}{\lambda}\right)\right] \operatorname{sinc}^2\left[\frac{b}{a}\left(m_y - \frac{RWFE_{P\text{-}Vy}[i,j]}{\lambda}\right)\right] \tag{2}$$

where λ is the design wavelength, m_x and m_y are the diffraction orders on x and on y, and $RWFE_{P\text{-}Vx}[i,j]$ and $RWFE_{P\text{-}Vy}[i,j]$ are the P-V RWFE values on x and on y at the pixel *[i, j]*, as defined in Equation (1). The term $\left(\frac{b}{a}\right)^4$ in Equation (2) represents the diffraction efficiency due to the amplitude part of the pupil function (the electronics shadow mask), and the sinc^2 terms represent the local diffraction efficiency on x and y caused by the phase part of the pupil function (the RWFE). The term $\frac{b}{a}$ in the argument of the two (sinc)^2 functions represents the truncation factor of the local P-V RWFE due to the limited active pixel width. For an SLM resolution of $N \times N$, the overall diffraction efficiency for any order can be calculated as the root-mean-square (RMS) across the entire pupil:

$$\sigma_{m_x,m_y} = \sqrt{\frac{\sum_{i,j=1}^{N}\left(\sigma_{m_x,m_y}[i,j]\right)^2}{N^2}} \tag{3}$$

In an FOS, wavefront aberrations at the ROI are corrected by the SLM, so diffraction becomes the dominant factor affecting the image quality at the ROI. The MTF of the FOS due to the amplitude diffraction can be written as

$$MTF_{diffr}(\xi) = \mathrm{tri}\left(\frac{\xi}{b/\lambda f}\right) * \left(\frac{\lambda f}{a}\right)^2 \mathrm{comb}^2\left(\frac{\xi}{a/\lambda f}\right) \times MTF_{aperture}(\xi) \tag{4}$$

where ξ is the spatial frequency, f is the focal length of the FOS, and $MTF_{aperture}(\xi)$ is the MTF of the aperture[22]. The left term in the expression from Equation (4) is a sawtooth function with the period $a/\lambda f$ and an average contrast of $\frac{b}{a}$. In the case of a high-resolution SLM, for $\xi > 0$, we can approximate the high-frequency sawtooth in Equation (4) by its average value, $\frac{b}{a}$. Since a portion of the light transmitted through the SLM will end up in higher diffraction orders, the MTF will be further affected by higher orders from other field angles falling onto the image plane. The images formed by the higher diffraction orders will superimpose onto the zero-order image, creating shifted "ghost" images of the extended object. The total amount of light diffracted from other field angles falling onto the zero-order at the ROI can be approximated by the total diffraction efficiency of the higher orders at the ROI[22]. The total transmission of all diffraction orders combined is equal to the fill factor, $\left(\frac{b}{a}\right)^2$. Therefore, the diffraction MTF in Equation (4) is washed down by a factor equal to $\frac{\sigma_{0,0}}{(b/a)^2}$. If we approximate the sawtooth in Equation (4) by its average value, $\frac{b}{a}$, for $\xi > 0$, the expression for the MTF at the ROI can be written as

$$MTF_{ROI}(\xi) = \frac{\sigma_{0,0}}{b/a} \times MTF_{aperture}(\xi) \tag{5}$$

Figure 2 shows the estimated MTF at the ROI for a diffraction-limited FOS with a circular aperture, an SLM pixel fill factor of $\left(\frac{b}{a}\right)^2$, and a zero-order diffraction efficiency at the ROI of $\sigma_{0,0}$.

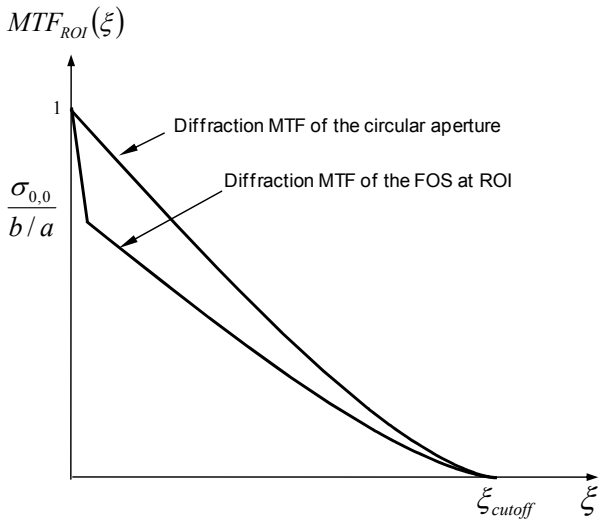

Figure 2: MTF at the ROI for a diffraction-limited FOS with a circular aperture.

4. DESIGN

Here we propose a very compact fast wide-angle FOS design, taking into account the current limitations in the transmissive TFT technology and their effects on the diffraction efficiency and MTF. We designed an 18 mm F/2.8 monochromatic lens for 532 nm that covers a full FOV of 80 degrees with a 25 mm diagonal sensor. The overall length of the optics is 33 mm, with a back focal length of 22 mm. The front negative element is a BK7 plano-concave spherical lens that can be manufactured by traditional grinding and polishing methods. The rear positive element is an SF57 bi-convex aspheric lens that can be manufactured by precision glass molding (PGM). The optical layout, wavefront aberration at 40 degrees, distortion, and relative illumination plots are shown in Figure 3. The RMS and P-V wavefront aberrations at 0º, 10º, 20º, 30º, and 40º are listed in Table 1.

Field angle in degrees	0º	10º	20º	30º	40º
RMS WFE in waves	1.82	1.29	1.10	1.67	1.19
P-V WFE in waves	6.47	4.69	6.03	8.28	8.40

Table 1: RMS and P-V wavefront aberrations of the uncorrected lens.

In a wide-angle FOS, the relative illumination (RI) should be flat in order to truly achieve uniform performance at the ROI across the entire FOV. A drop in the RI with the field angle would result in a lower MTF contrast at the peripheral field angles. In this design, the RI drops only by 12% at the corner. It is difficult to flatten the RI and correct the barrel distortion in the same time. However, distortion is only a field-dependent magnification error, and does not affect the resolution of the optics. As long as the resolution of the sensor array is large enough to avoid aliasing due to under-sampling, barrel distortion can be calibrated and corrected at the electronics or software level. The barrel distortion is 24% at the maximum field angle.

The resolution of the transmissive LC SLM has to be carefully selected in order to optimize the FOS performance. If the SLM resolution is too low, the RWFE will affect the diffraction efficiency and MTF of the system. On the other hand, since the minimum shadow mask width is limited by the current TFT technology, increasing the SLM resolution for a given aperture size will decrease the fill factor, also affecting the diffraction efficiency and MTF. Therefore, choosing the optimal SLM resolution is a tradeoff between minimizing the amplitude diffraction effects caused by the shadow mask, and minimizing the phase diffraction effects caused by the RWFE.

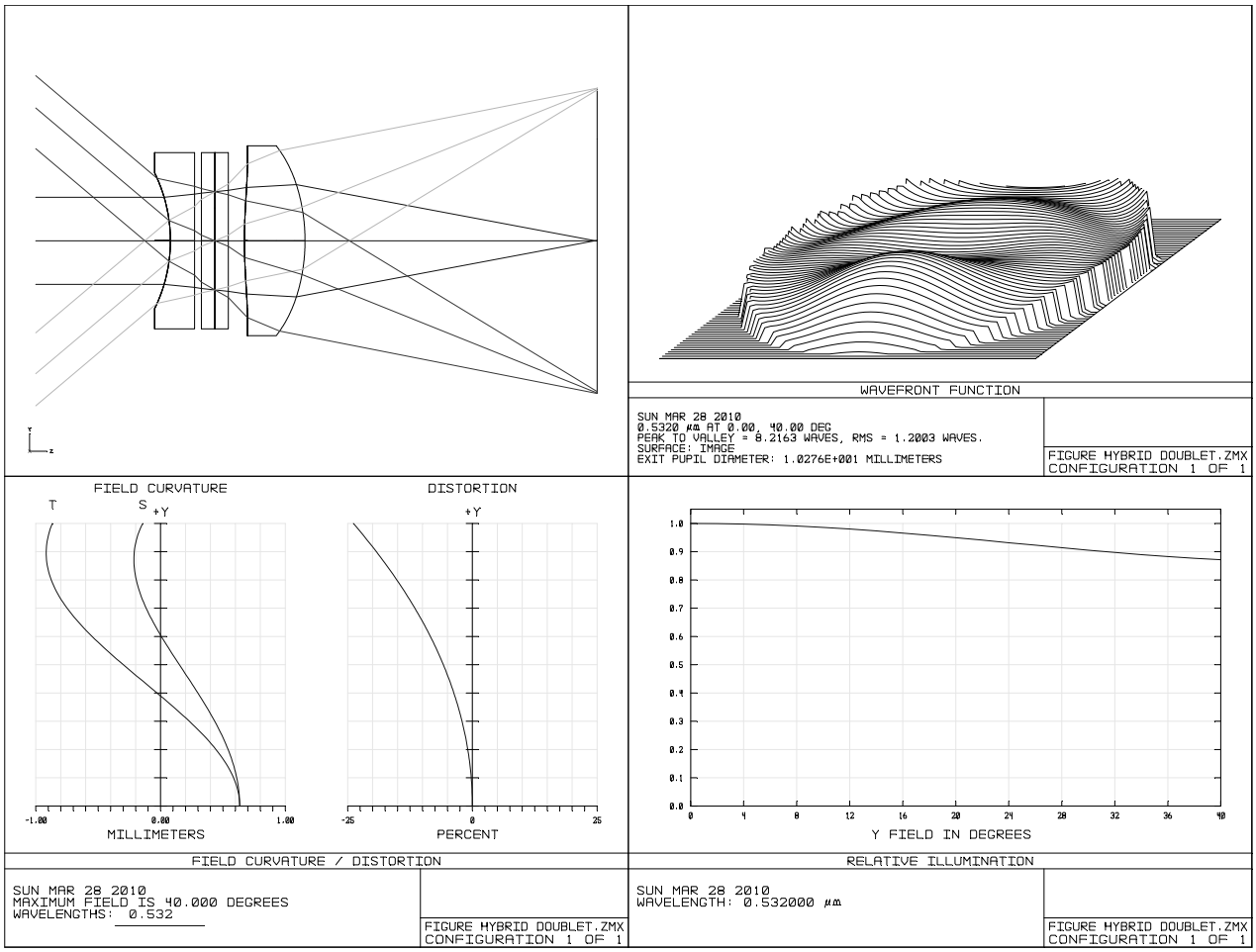

Figure 3: Optical layout, wavefront aberration at 40 degrees, distortion, and relative illumination plots.

In this design, the SLM resolution was optimized based on the largest P-V wavefront aberration, which occurs at the 40º field angle. The two-dimensional wavefront aberration map at the 40º field angle was obtained directly from Zemax. The values for the local P-V RWFE on x and y at each pixel $[i, j]$, $RWFE_{P\text{-}Vx,y}[i, j]$, as defined in Equation (1), were determined from the wavefront map, for five different SLM resolution scenarios: 32×32, 64×64, 128×128, 256×256, and 512×512. For an SLM resolution of $N \times N$, the ratio $\frac{b}{a}$ can be calculated as

$$\frac{b}{a} = 1 - \frac{w}{a} = 1 - \frac{N w}{D_{Stop}} \tag{6}$$

where w is the width of the shadow mask and D_{Stop} is the pupil stop diameter. In this design, $D_{Stop} = 7.24$ mm, and we considered $w = 2.8$ µm, which is the smallest shadow mask width that can be currently achieved in the transmissive TFT technology. The $\frac{b}{a}$ values obtained from Equation (6) and the $RWFE_{P\text{-}Vx,y}[i, j]$ values obtained from the wavefront map were used in Equations (2) and (3) to calculate the zero-order diffraction efficiency, $\sigma_{0,0}$. The MTF at $\xi = 0+$ was calculated as $\frac{\sigma_{0,0}}{b/a}$. Table 2 lists the pixel pitch, fill-factor, $\sigma_{0,0}$, and $MTF(\xi = 0+)$, for the five different SLM

resolutions considered, with the ROI at 40º. The optimal SLM resolution for this FOS design example is 128×128. For lower SLM resolutions, the phase diffraction caused by the RWFE is the main factor limiting the diffraction efficiency and the image quality at the ROI. For higher SLM resolutions, the amplitude diffraction caused by the shadow mask becomes the dominant factor affecting the performance of the FOS at the ROI.

SLM resolution	32×32	64×64	128×128	256×256	512×512
Pixel pitch [μm]	226	113	57	28	14
Fill factor	0.98	0.95	0.90	0.81	0.64
$\sigma_{0,0}$	0.62	0.76	0.76	0.64	0.41
$MTF(\xi = 0+)$	0.62	0.78	0.80	0.72	0.51

Table 2: Performance at the ROI with five different SLM resolutions (ROI at 40º).

The zero-order diffraction efficiency and $MTF(\xi = 0+)$ at the ROI were also calculated with the correction applied at 0º, 10º, 20º, and 30º, for an SLM resolution of 128×128 (listed in Table 3). Notice that the performance at the ROI is almost uniform across the entire FOV, a result of the wavefront aberration being distributed somewhat evenly over the FOV.

Field angle in degrees	0º	10º	20º	30º	40º
$\sigma_{0,0}$	0.78	0.78	0.76	0.75	0.76
$MTF(\xi = 0+)$	0.82	0.82	0.80	0.79	0.80

Table 3: Performance with correction applied at 40º (128×128 SLM resolution).

But what happens at the other field angles when the wavefront aberration is corrected at the ROI? The diffraction efficiency at any given field angle is affected only by the initial wavefront aberration at that particular field angle, and remains constant regardless of where within the FOV the correction is applied. However, in addition to the amplitude and phase diffraction effects caused by the pixelated structure of the SLM, these field angles are also affected by the uncorrected wavefront aberration, $W - W_{ROI}$, where W is the initial aberration and W_{ROI} is the wavefront correction applied at the ROI. Figure 4 shows the estimated MTF of the FOS with the wavefront aberration corrected at 40º. Notice that, only 1º away from the ROI, at the 39º field angle, the MTF drops significantly. Since aberrations in fast wide-angle lenses change rapidly with the field angle, aberrations become the dominant factor affecting the image quality away from the ROI.

At the ROI, the contrast at 300 lp/mm is 37%. Therefore, this FOS can be used with a foveated CMOS sensor array having a Nyquist frequency of 300 lp/mm, which corresponds to a 1.7 μm pixel pitch. A 25 mm diagonal sensor with 1.7 μm pixels would have a resolution of 108 MPixel. This large resolution would require foveated imaging based on CMOS active sensors to transmit video frames in real-time. At 1º away from the ROI, the resolution drops by about a factor 6×6, and further away, across the rest of the FOV, the resolution drops by as much as a factor 20×20. In this case, the CMOS foveated sensor would have to be designed such that it would only capture and transmit full-resolution images within a small local FOV (less than 1º) around the ROI. Away from the ROI active pixel binning can be applied by combining the signal from as many as 400 pixels. Such a foveated imaging system would be capable of capturing and transmitting very high-resolution images at the ROI in real time while covering a large FOV.

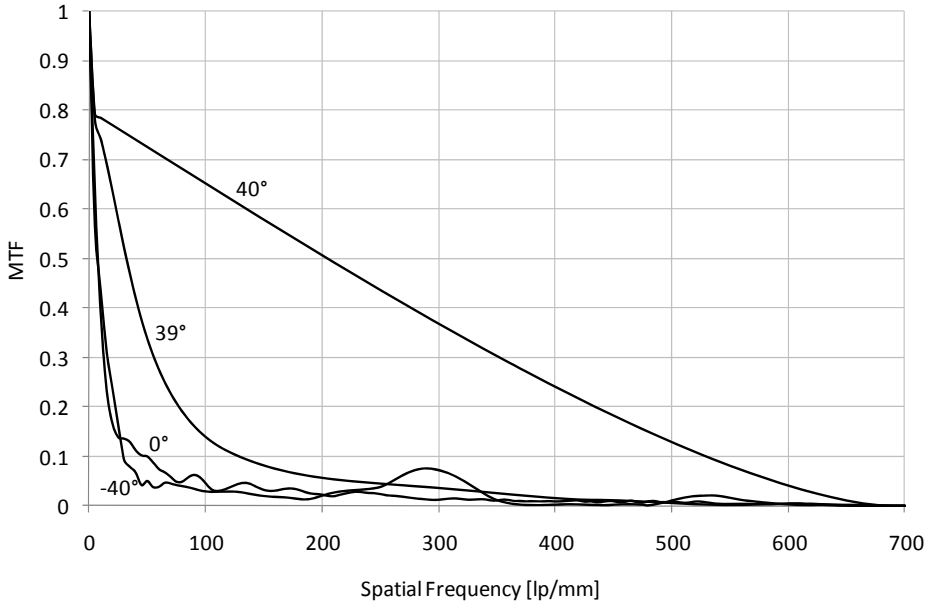

Figure 4: MTF of the FOS with the aberrations corrected at 40 degrees.

5. TOLERANCE ANALYSIS

There are three main factors affecting the image quality in optical systems: diffraction, aberrations left uncorrected by design, and additional aberrations caused by fabrication and assembly errors. So far, we have only taken into consideration the first two factors, ignoring the aberrations caused by the fabrication and assembly errors. However, although tolerances might not have a major impact on the image quality of slow optical systems, they can significantly affect the final performance of the manufactured lenses in the case of fast optical systems. Well-corrected fast lenses can be very sensitive to fabrication and assembly errors. In general, designs with relatively large incidence angles at an optical surface are sensitive to errors in that particular surface. Since fast wide-angle lenses designed to be used in FOSs only have a limited number of elements, marginal rays in the pupil and rays in the peripheral fields typically end up having rather large incidence angles at the optical surfaces. As a result, these lenses tend to be very sensitive to fabrication and assembly errors.

In order to analyze the effect of fabrication and assembly tolerances on the image quality of our FOS design, we ran a Monte-Carlo (MC) tolerance analysis with the tolerances listed in Table 4. These tolerances are relatively tight for the 15 mm diameter optics in this design, but can be achieved by most optical fabrication shops. The merit function criterion for the MC tolerance analysis was set to be the RMS wavefront aberration at 40º with the nominal wavefront correction applied at 40º (nominal wavefront error is zero). The analysis was run with 100 random trials using a normal distribution for the manufacturing errors, without adjusting the focus or any other mechanical compensators. A random MC trial with the merit function close to the 50% percentile margin was chosen to model a typical manufactured lens. Figure 5 shows the MTF of this "as manufactured" FOS with the nominal aberration corrected at 40º, without SLM compensation for additional fabrication and assembly errors. The drop in the MTF at the ROI due to manufacturing errors is significant compared to the nominal diffraction-limited MTF. In other words, if the SLM of this fast wide-angle FOS would be programmed to correct the aberrations obtained from the nominal lens design, the manufactured FOS will not have the expected diffraction-limited image quality at the ROI.

Surface power/irregularity	2/1 fringes
Glass CT	± 0.020 mm
Element wedge	< 1.8 arcmin
Refractive index	± 0.0001
Air CT	± 0.020 mm
Element tilt	± 1.2 arcmin
Element centration	± 0.020 mm

Table 4: Performance at the ROI with five different SLM resolutions (ROI at 40º).

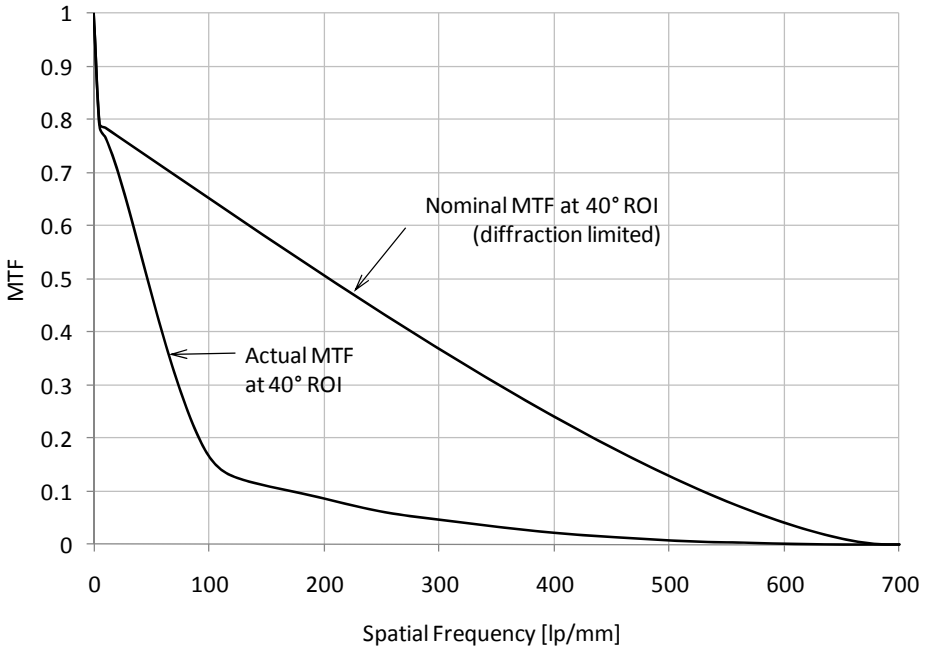

Figure 5: MTF with the ROI at 40º without compensation for additional aberrations caused by fabrication and assembly errors.

On the other hand, a great advantage of FOSs is that, besides correcting the nominal wavefront aberrations, these systems also have the ability to correct any additional aberrations introduced by fabrication and assembly errors. The FOS can be calibrated by measuring the actual wavefront of the manufactured lens and reprogramming the SLM to eliminate any additional aberrations. However, the aberrations introduced by fabrication and assembly errors are not rotationally symmetric with respect to the optical axis, and they also might vary quickly with the field angle in fast wide-angle lenses. As a result, in order to obtain diffraction-limited image quality at the ROI across the entire FOV, a fast wide-angle FOS would have to be calibrated at several field angles within the FOV.

6. EQUIVALENT CONVENTIONAL LENSES

The zero-order diffraction efficiency in the FOS design example developed here is roughly 76%. From a radiometric point of view, a transmission loss is equivalent to closing down the aperture of the lens. Since the transmission of a lens is proportional to $(1/F/\#)^2$, our F/2.8 FOS is equivalent to an F/3.2 conventional lens in terms of transmission,

assuming a polarization-independent SLM with no additional transmission losses. An F/3.2 lens would be less aberrated than an F/2.8 lens, which leads to the inevitable question whether optical foveated imaging based on the current transmissive LC SLM technology has any major advantage over conventional wide FOV imaging optics. Therefore, we thought it would be interesting to design two different equivalent conventional F/3.2 lenses, with the same focal length and FOV as the FOS, and compare them to the FOS in terms of their size and image quality (MTF).

The first equivalent conventional lens is an all-spherical 7-element design optimized for almost diffraction-limited performance across the entire FOV. At the expense of a much more complex and bulky design, this lens has an image quality across the entire FOV comparable to the image quality of the FOS at the ROI. The second equivalent conventional lens is a two-element design obtained by closing down the aperture and reoptimizing the F/2.8 design used for the FOS, while maintaining the same configuration: spherical plano-concave negative element followed by an aspheric bi-convex positive element. This second lens is comparable in size and complexity to the FOS, but the image quality is relatively poor. To compare MTF curves, the FOS was assumed to be calibrated across the entire FOV to achieve diffraction-limited performance, and the effect of fabrication and assembly tolerances was not taken into consideration for the conventional lenses (nominal MTF shown). Figure 6 (a) compares the MTF of the FOS at the ROI to the MTF curves of the equivalent conventional lenses at 0º, 10º, 20º, 30º, and 40º. Figure 6 (b) compares the relative sizes of the conventional lenses to the size of the FOS. In this case, the FOS fits in a cylinder with a volume 27 times smaller than the volume of the well-corrected equivalent conventional lens, which is a significant reduction in size. A side-by-side comparison between the FOS and the conventional lenses is listed in Table 5.

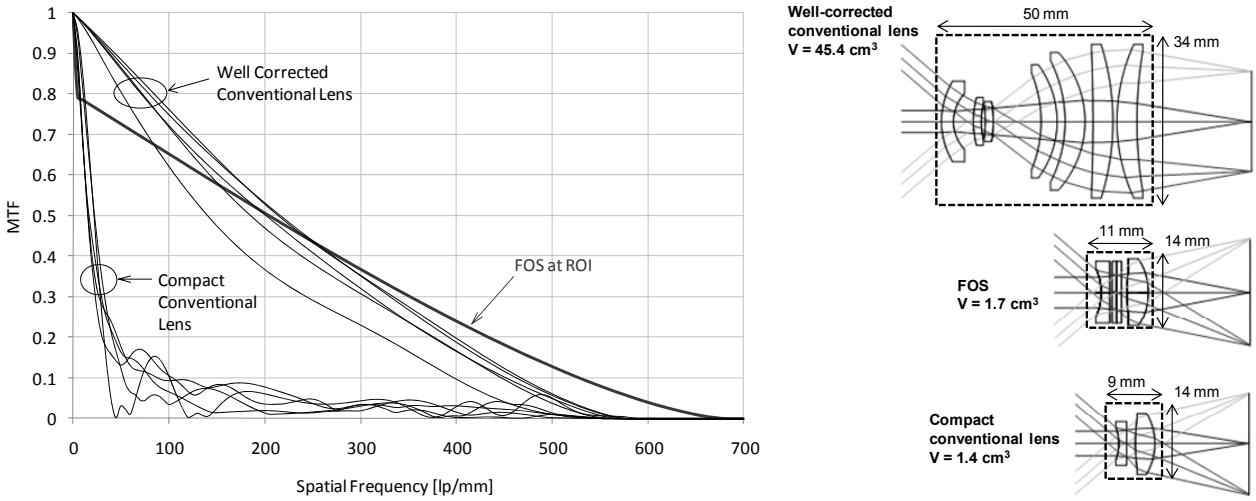

(a) (b)

Figure 6: (a) MTF of the FOS at the ROI versus MTF curves of equivalent conventional lenses. (b) Size of the FOS compared to the size of the equivalent conventional lenses.

Lens	FOS	Compact conventional lens	Well-corrected conventional lens
MTF at 300 lp/mm	37%	n/a	32%
Resolution [MPixel]	100	1	100
Volume [cm^3]	1.7	1.4	45.4

Table 5: Performance with correction applied at 40º (128×128 SLM resolution).

7. SUMMARY

We presented a theoretical model to estimate diffraction efficiency and MTF of an FOS by quantifying the amplitude and phase diffraction effects caused by the pixelated aperture of the SLM. This model can be used as a design and optimization tool for the development of future wide-angle FOSs. Our model reveals limitations imposed by the current transmissive LC SLM technology: the shadow mask and discrete piston-only OPD are the main factors affecting performance at the ROI. Diffractive effects limit the amount of wavefront aberration that can be efficiently corrected using transmissive LC SLMs.

We also proposed a very compact fast wide-angle lens design that can be used to build high-resolution FOSs based on the current technology. The main design challenges were controlling the relative illumination, distortion, and distribution of aberrations across a wide FOV with a limited number of elements. We also showed that choosing the optimal SLM resolution for a given lens design is a tradeoff between minimizing amplitude diffraction effects caused by the shadow mask and minimizing phase diffraction effects caused by the discrete piston−only correction. Such an FOS would be capable of capturing very high-resolution images at the ROI while covering a relatively large FOV. The reduction in volume of the FOS compared to an equivalent conventional lens of equal image quality is remarkable.

Custom parts, such as foveated CMOS sensors, optics, and SLMs would have to be developed in order to achieve compact systems capable of unprecedented performance. Future developments include: develop polarization-independent transmissive SLM devices, further decrease shadow mask width in transmissive SLMs, develop high-resolution foveated active CMOS sensors, and develop an automatic calibration setup to evaluate aberrations caused by manufacturing errors and reprogram the SLM.

REFERENCES

1. N. Tsumura, C. Endo, H. Haneishi, and Y. Miyake, “Image compression and decompression based on gazing area,” *Proc. SPIE* **2657**, 361-367 (1996).
2. P. Kortum and W. Geisler, “Implementation of a foveated image coding system for image bandwidth reduction,” *Proc. SPIE* **2657**, 350-360 (1996).
3. W. S. Geisler and J. S. Perry, “A real-time foveated multi-resolution system for low-bandwidth video communication,” *Proc. SPIE* **3299**, 294-305 (1998).
4. A. Ude, C. Gaskett, and G. Cheng, “Foveated vision systems with two cameras per eye,” *Proc. IEEE, International Conference on Robotics and Automation*, 3457-3462 (2006).
5. H. Hua and S. Lin, “Dual-sensor foveated imaging system,” *Appl. Opt.* **47**(3), 317-327 (2008).
6. Z. Zhou, B. Pain, and E. R. Fossum, “Frame-transfer CMOS active pixel sensor with pixel binning,” *IEEE Transactions on Electron Devices* **44(**10), 1764-1768 (1997).
7. J. Coulombe, M. Swan, and C. Wang, “Variable resolution CMOS current mode active pixel sensor,” *Proc. IEEE, International Symposium on Circuits and Systems 2000,* Vol. 2, 293-296 (2000).
8. F. Saffih and R. Hornsey, “Multiresolution CMOS image sensor,” *Tech. Digest SPIE, Opto-Canada 2002*, 425 (2002).
9. K. Wakamiya, T. Senga, K. Isagi, N. Yamamura, Y. Ushio, and N. Kita, “A new foveated wide angle lens with high resolving power and without brightness loss in the periphery,” *Proc. SPIE* **6051**, 605107-1-10 (2005).
10. T. Martinez, D. V. Wick, and S. R. Restaino, “Foveated, wide field-of-view imaging system using a liquid crystal spatial light modulator,” *Opt. Express* **8**(10), 555-560 (2001).
11. D. V. Wick, T. Martinez, S. R. Restaino, and B. R. Stone, “Foveated imaging demonstration,” *Opt. Express* **10**(1), 60-65 (2002).
12. G. Curatu, D. V. Wick, D. M. Payne, T. Martinez, J. Harriman, and J. E. Harvey, “Wide field-of-view imaging system using a liquid crystal spatial light modulator,” *Proc. SPIE* **5874**, 587408-1-7 (2005).
13. G. D. Love, “Wave-front correction and production of Zernike modes with a liquid-crystal spatial light modulator,” *Appl. Opt.* **36**(7), 1517-1524 (1997).

14. J. Harriman, S. Gauza, S-T. Wu, D. V. Wick, B. Bagwell, T. Martinez, D. M. Payne, and S. Serati, "Transmissive spatial light modulators with high figure-of-merit liquid crystals for foveated imaging applications," *Proc. SPIE* **6135**, 61350C-1-13 (2006).
15. B. E. Bagwell, D. V. Wick, and J. Schwiegerling, "Multi-spectral foveated imaging system," *Proc. IEEE, Aerospace Conference 2006*, 1114 (2006).
16. B. E. Bagwell, D. V. Wick, R. Batchko, J. D. Mansell, T. Martinez, S. R. Restaino, D. M. Payne, J. Harriman, S. Serati, G. Sharp, and J. Schwiegerling, "Liquid crystal based active optics," *Proc. SPIE* **6289**, 628908 (2006).
17. D. V. Wick, D. M. Payne, T. Martinez, and S. R. Restaino, "Large dynamic range wavefront control of micromachined deformable membrane mirrors," *Proc. SPIE* **5798**, 158-161 (2005).
18. J. Harriman, S. Serati, and J. Stockley, "Comparison of transmissive and reflective spatial light modulators for optical manipulation applications," *Proc. SPIE* **5930**, 59302D-1-10 (2005).
19. M. T. Gruneisen, R. C. Dymale, J. R. Rotgé, D. G. Voelz, and M. Deramo, "Wavelength-agile telescope system with diffractive wavefront control and acusto-optic spectral filter," *Opt. Eng.* **44**(10), 103202-1-5 (2005).
20. B. E. Bagwell, D. V. Wick, W. D. Cowan, O. B. Spahn, W. C. Sweatt, T. Martinez, S. R. Restaino, J. R. Andrews, C. C. Wilcox, D. M. Payne, and R. Romeo, "Active zoom imaging for operationally responsive space," *Proc. SPIE* **6467**, 64670D-1-8 (2007).
21. X. Zhao, "Broadband and wide field of view foveated imaging system in space," *Opt. Eng.* **47**(10), 103202-1-5 (2008).
22. G. Curatu and J. E. Harvey, "Analysis and design of wide-angle foveated optical systems based on transmissive liquid crystal spatial light modulators," *Opt. Eng.* **48**(4), 043001-1-11 (2009).